

Topological States in Generalized Electric Quadrupole Insulators

Chang-An Li^{1,2} and Shu-Shan Wu³

¹*School of Science, Westlake University, 18 Shilongshan Road, Hangzhou 310024, Zhejiang, China*

²*Institute of Natural Sciences, Westlake Institute for Advanced Study,
18 Shilongshan Road, Hangzhou 310024, Zhejiang, China*

³*Department of Physics, Hangzhou Normal University, Hangzhou 310036, Zhejiang, China*

(Dated: January 27, 2023)

The theory of electric polarization has recently been extended to higher multipole moments, such as quadrupole and octupole moments. The higher electric multipole insulators in their essence are topological crystalline phases protected by underlying spatial symmetries. Henceforth, it is natural to ask what are the consequences of symmetry breaking, including both spatial and nonspatial symmetry breaking, in these multipole insulators. In this paper, we investigate topological phases of generalized electric quadrupole insulators. Explicitly, we generalize the Benalcazar-Bernevig-Hughes model by adding specific terms to break spatial as well as nonspatial symmetries. It is found that the believed topological equivalence between Wannier bands and edge spectrum can be invalid in simple generalized models. And the nested Wilson loop approach may not be universally suitable to characterize high-order topology in higher electric multipole insulators. Furthermore, it is shown that the quadrupole moments can remain quantized even mirror symmetries are absent or there is strong disorder presented in the system.

I. INTRODUCTION

Electric polarization in crystalline was once a long-standing issue since it is not a well-defined observable that can simply be given by expectation value of a position operator. Actually, only its derivative with respect to some parameters is a measurable quantity [1, 2]. The modern theory of bulk polarization is based on Berry phase, which is calculated with wave functions of energy bands over a closed path in Brillouin zone [3]. The theory has wide and deep impacts on condensed matter physics in recent decades, especially on the development of topological band insulators [4–7]; for instance, a varying of electric polarization under an adiabatic cycle is associated with Chern number [8], which is recognized as one of the most fundamental indexes in topological phases of matter, and in the same spirit, the time-reversal polarization gives rise to Z_2 index of topological insulators [9].

Recent research extends the modern theory of polarization to higher multipole moments, such as quadrupole and octupole moments. As is well known, quantized bulk polarization in Su-Schrieffer-Hegger (SSH) model gives rise to fractional charge $\pm e/2$ at the boundaries of one-dimensional sample [10]. Benalcazar *et al.* extended the similar idea to two-, and three-dimensional systems which hold quantized bulk quadrupole and octupole moments, respectively [11, 12]. As such, these systems are dubbed electric quadrupole and octupole insulators. It is shown by explicit models that these quantized bulk multipole moments also manifest fractionalized boundary charges. While here the bulk-boundary correspondence is different from the conventional topological insulators. Traditionally, a topological bulk state in d -dimension has robust $d - 1$ dimensional boundary states. Nevertheless,

topological quadrupole (octupole) insulators have localized states at corners, which are $d - 2$ ($d - 3$) boundaries of the system. This “high-order” bulk-boundary correspondence [13] casts these topological phases into a new class of topological insulators called “high-order topological insulators” [14]. Generally, a d -dimensional high-order topological insulator has nontrivial boundary states at $d - m$ boundary ($m \geq 2$). The high-order topological insulators have consequently attracted both theoretical and experimental interest over past years [15–24], and have been extended to high-order topological superconductors [25–31] and even semimetals [32–34].

The higher electric multipole insulators in their essence are topological crystalline insulators [35, 36], and the quantization of multipole moments is imposed by certain underlying spatial symmetries of the system. For example, in the proposed Benalcazar-Bernevig-Hughes (BBH) model, the quantization of quadrupole (octupole) moments are promised by a combination of mirror symmetries [12]. Apart from spatial symmetries, high-order topological insulators may also need some of nonspatial symmetries, namely, chiral, time-reversal, and particle-hole symmetry, to protect their high-order topology [14, 37, 38]. It is natural to ask what are the consequences of symmetry breaking, including nonspatial and even spatial symmetry breaking, in higher electric multipole insulators. Naively speaking, spatial symmetry breaking can ruin their topological phases while the nonspatial symmetry breaking is irrelevant. However, the consequences are not such straightforward. Besides, the high-order topology in BBH model is characterized by so-called “nested Wilson loop”. This characterization is based on the fact that there is equivalent topology between Wannier bands and edge spectrum [39–42]. The equivalence, however, may be lost under certain circum-

stances [43, 44]. If in that case, it is also meaningful to ask how to demonstrate high-order phase if nested Wilson loop approach fails.

In the present paper, we mainly exploit three different generalized BBH models to study newly appearing topological phases and the consequences of symmetry breaking in electric quadrupole insulators, and also study the effect of disorder on the original BBH model. In the first generalized model, we add additional hopping terms to break chiral symmetry. As the prototype base of BBH model is SSH model, these chiral symmetry breaking terms lead the system to an indirect gap phase. Quadrupole moments will be buried (or ill-defined) by bulk bands, nevertheless the nested Wilson loop approach fails to capture this phase since there is no real topological phase transition. In the second model, we add imaginary hopping terms to break time-reversal and chiral symmetries. The equivalent topology between Wannier bands and edge spectrum could be lost in this simple model after an induced phase transition. In that case, the nested Wilson loop approach is no longer applicable since its basis is ruined, while the quantized quadrupole moments together with edge polarization and fractional corner charges remain good signatures to characterize high-order topology. In the third model, we focus on mirror symmetry breaking, and keep inversion symmetry to have well-defined quadrupole moments at the mean time. Unexpectedly, the quadrupole moments remain quantized even mirror symmetry is ruined. More interestingly, we find the quantized quadrupole moments are even robust against strong disorders added to the system.

The remainder of this paper is organized as follows. Section II briefly reviews the BBH model for the convenience of our subsequent discussion. Section III introduces the extended model with chiral symmetry breaking, and discusses the appearance of indirect gap phase. Section IV provides the model with time-reversal and chiral symmetry breaking. In Section V, the consequence of mirror symmetry breaking is detailed. Section VI considers the robustness of quantized quadrupole moments in the presence of disorders. Finally, we conclude our results with a discussion in Section VII.

II. OVERVIEW OF BENALCAZAR-BERNEVIG-HUGHES MODEL

For the convenience of our discussion about generalized models in the subsequent sections, let us first briefly review the BBH model [11, 12] in two-dimension (2D). The tight-binding Hamiltonian in real space is described as

$$H_0 = \sum_{\mathbf{R}} \left[\gamma_x (C_{\mathbf{R},1}^\dagger C_{\mathbf{R},3} + C_{\mathbf{R},2}^\dagger C_{\mathbf{R},4}) + \gamma_y (C_{\mathbf{R},1}^\dagger C_{\mathbf{R},4} - C_{\mathbf{R},2}^\dagger C_{\mathbf{R},3}) + \lambda (C_{\mathbf{R},1}^\dagger C_{\mathbf{R}+\hat{x},3} + C_{\mathbf{R},4}^\dagger C_{\mathbf{R}+\hat{x},2}) + \lambda (C_{\mathbf{R},1}^\dagger C_{\mathbf{R}+\hat{y},4} - C_{\mathbf{R},3}^\dagger C_{\mathbf{R}+\hat{y},2}) \right] + H.c., \quad (1)$$

where $C_{\mathbf{R},\zeta}^\dagger$ ($C_{\mathbf{R},\zeta}$) are creation (annihilation) operators at unit cell $\mathbf{R} = (m\hat{x}, n\hat{y})$ with $\zeta = 1, 2, 3, 4$ being orbital-like degree of freedoms. Here the parameters $\gamma_{x,y}$ and λ are hopping amplitudes within and between unit cells, as sketched in the Fig. 1(a). Note the lattice constant is assumed to be unity throughout the following. The corresponding Bloch Hamiltonian is

$$H_q(\mathbf{k}) = [\gamma_x + \lambda \cos k_x] \Gamma_4 + \lambda \sin k_x \Gamma_3 + [\gamma_y + \lambda \cos k_y] \Gamma_2 + \lambda \sin k_y \Gamma_1. \quad (2)$$

The Gamma matrices are defined as $\Gamma_j = -\tau_2 \sigma_j$, and $\Gamma_4 = \tau_1 \sigma_0$ with τ and σ both being Pauli matrices for the unit cell orbital degrees of freedom. The bulk bands of Eq. 2 are gapped unless $\gamma_s/\lambda = \pm 1$ ($s = x, y$). Hence it is an insulator at half-filling. The model gives rise to topological quadrupole moments protected by mirror symmetries in principle. The nonspatial symmetries preserved are chiral symmetry \mathcal{C} , time-reversal symmetry \mathcal{T} , and particle-hole symmetry \mathcal{P} , although they are not necessarily needed to quantize quadrupole moments.

The topological phase in electric quadrupole insulators is characterized by quantized quadrupole moments $q_{xy} = 0, 1/2$, which induce corner charge Q^{corner} and edge polarization p^{edge} of its equal magnitude. The quantization of q_{xy} is promised by mirror symmetries in principle. Explicitly, the quantized quadrupole moments are formulated via the nested Wilson loops approach. The electric quadrupole insulators in 2D have boundaries that are stand-alone 1D topological insulators. Sitting on the basis that Wannier bands and boundary spectrum are topologically equivalent, the topological quadrupole phase is characterized by Wannier sector polarization $\mathbf{p}^\nu \equiv (p_y^{\nu_x}, p_x^{\nu_y})$. The nontrivial topological quadrupole phase constrains parameter region $|\gamma_s/\lambda| < 1$ for $s = x, y$ [12]. In the following we set $\lambda = 1$ otherwise specified.

III. INDIRECT GAP PHASES: CHIRAL SYMMETRY BREAKING

The BBH model is based on SSH model, whose topology is protected by chiral symmetry. Thus in this section we consider a generalized BBH model with chiral symmetry breaking by introducing hopping terms between equivalent sites as sketched in Fig. 1(a). The dressed model is

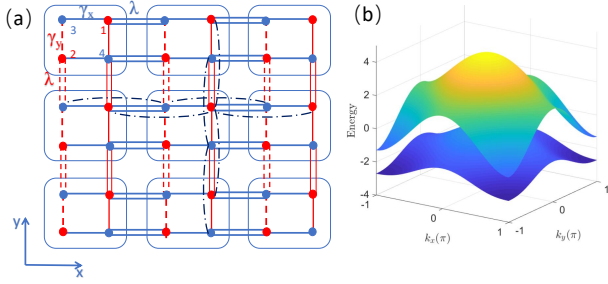


Figure 1. (a) Lattice structure of extended BBH model H_1 . The dashed dark blue lines represent hopping at equivalent sites with strength t between nearest unit cells. For simplicity, here we only sketch parts of this kind of hopping. (b) Energy bands corresponding to (a) with parameters fixed at $\gamma_x = \gamma_y = 0.5$, and $t = 0.5$. Here the system has indirect gap.

$$H_1 = H_0 + \sum_{\mathbf{R}} \sum_{\zeta=1}^4 \sum_{s=x,y} t(C_{\mathbf{R},\zeta}^\dagger C_{\mathbf{R}+\hat{s},\zeta} + H.c.), \quad (3)$$

where t is the corresponding hopping amplitude. In the momentum space, the corresponding Bloch Hamiltonian reads

$$H_1(\mathbf{k}) = H_q(\mathbf{k}) + 2t \sum_{s=x,y} \cos k_s. \quad (4)$$

Due to the appearance of identity terms in Eq. 4, chiral symmetry is no longer preserved. One can check that

$$\mathcal{C}H_1(\mathbf{k})\mathcal{C}^{-1} \neq -H_1(\mathbf{k}), \quad \mathcal{C} = \tau_3\sigma_0. \quad (5)$$

Particle-hole symmetry is not preserved either, which is obvious from the energy spectrums

$$E_{\pm} = 2t \sum_{s=x,y} \cos k_s \pm \sqrt{\epsilon_x^2(k_x) + \epsilon_y^2(k_y)}, \quad (6)$$

where $\epsilon_s^2(k_s) = \gamma_s^2 + 2\gamma_s\lambda \cos k_s + \lambda^2$. While the energy bands are still doubly degenerated since time-reversal and inversion symmetries are both respected. The global symmetries cast the system into AI class, and its classification is trivial in 2D [45, 46]. Note the additional term in Eq. 4 keeps mirror symmetries $\mathcal{M}_{x,y}$ of Hamiltonian.

The appearing new “phase” is an indirect gap phase due to chiral symmetry breaking [47–49]. Note by inspection of Fig. 1(b), the maximum point of valence band E_{\max}^V exceeds the minimum value of conduction bands E_{\min}^C , but there is no bulk gap closure. Here we dub this phase as indirect gap phase. The condition for the appearance of indirect gap phase is determined by the inequality

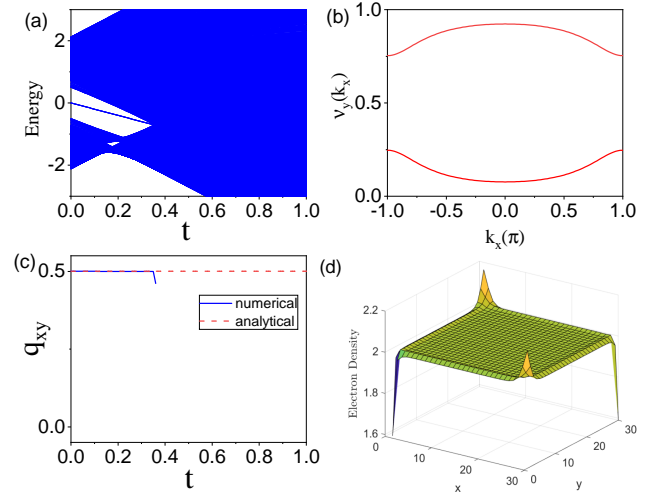


Figure 2. Indirect gap phase induced by chiral symmetry breaking. (a) Energy spectrum of H_1 as functions of t . (b) Wannier bands for fixed $t = 0.5$. (c) Calculated quadrupole moments when varying t (red line is calculated analytically with nested Wilson loop approach, blue line is calculated numerically under periodic boundary condition with size 40×40). (d) Electron charge density in the nontrivial phase with $t = 0.2$. Other parameters are set at $\gamma_x = \gamma_y = 0.5$.

$$t > \frac{1}{8} \sum_{\alpha=\pm} \sqrt{\sum_{s=x,y} (\gamma_s + \alpha\lambda)^2}. \quad (7)$$

The indirect gap phase buries quadrupole moments, while this drastic change is not reflected by the Wannier sector polarization since \mathbf{p}^ν always insists the original value at $t = 0$ regardless of the varying of t . It is shown in Fig. 2(b) that the Wannier band are not affected by increasing t , either. This is reasonable since no gap closure process takes place and the eigen states are unchanged.

There is a real space recipe to obtain the electric quadrupole moments [50, 51]. It is calculated as

$$q_{xy} = \frac{1}{2\pi} \text{Im} \log \langle \Psi_G | \hat{U}_2 | \Psi_G \rangle, \quad (8)$$

where $|\Psi_G\rangle$ is the many-body ground states, and $\hat{U}_2 \equiv \exp[i2\pi\hat{q}_{xy}]$ with $\hat{q}_{xy} = \sum_{\mathbf{R}} xy\hat{n}(\mathbf{R})/(L_x L_y)$ being quadrupole momentum density operator per unit cell at position \mathbf{R} . Here $L_{s=x,y}$ are the length of sample along s direction. Note that we need to eliminate the contribution from atomic limit [52]. Although it still has some defects [53], this recipe turns out to be useful. Note that the formula is applied under periodic boundary conditions.

It is clear that the nontrivial regions will shrink due to appearance of indirect gap phase. Let us revisit Figs. 2(a) and 2(c). Before entering the indirect gap phase, the

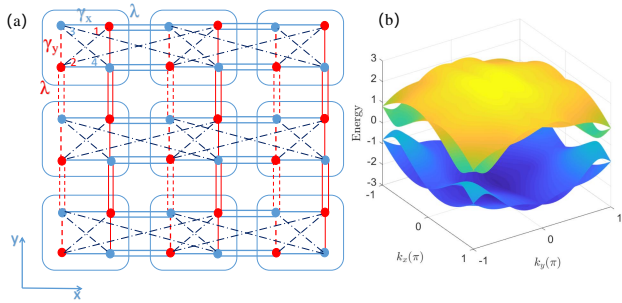


Figure 3. (a) Lattice structure of extended BBH model H_2 . The dashed dark blue lines represent hopping within and between unit cells. These hopping with imaginary amplitudes will break time-reversal symmetry. (b) Energy bands corresponding to (a) with parameters fixed at $\gamma_x = 0.8$, $\gamma_y = 0.5$, and $J_2 = 0.3$. The band degeneracy is lifted.

quantized quadrupole moments $q_{xy} = 1/2$ remains, accompanied by the sharply localized corner state, but its corresponding energy is shifted away from zero-energy. Seen from Fig. 2(d), the charge density is not “symmetric” with respect to different corners, but the integrated charge over a quarter of sample around each corner still quantizes to $\pm e/2$. After the “transition” point, the corner states are hidden by bulk valence bands, and the quantized quadrupole moments are ruined. The buried corner states work similarly as hidden edge states in topological insulators [54, 55]. At this case, the system has no gap thus the real space recipe is not applicable.

IV. DISCREPANT TOPOLOGY BETWEEN WANNIER BANDS AND EDGE SPECTRUM

In this section, we investigate the consequences of non-spatial symmetry breaking (time-reversal and chiral symmetry) in another generalized BBH model. The imaginary hopping terms are introduced as shown in Fig. 3(a). The corresponding modified Hamiltonian is

$$H_2 = H_0 + \sum_{\mathbf{R}} J_2 (iC_{\mathbf{R},2}^\dagger C_{\mathbf{R},1} - iC_{\mathbf{R},4}^\dagger C_{\mathbf{R},3} + H.c.) + \sum_{\mathbf{R}} J_2 (-iC_{\mathbf{R},2}^\dagger C_{\mathbf{R}+\hat{x},1} - iC_{\mathbf{R},3}^\dagger C_{\mathbf{R}+\hat{x},4} + H.c.), \quad (9)$$

where iJ_2 is the hopping amplitude. It is imaginary due to half π -flux enclosed and the sign convention is as in Eq. 9. These imaginary hopping terms break time-reversal symmetry, like Haldane model, [56]. For simplicity, only iJ_2 hopping along x direction is considered, and we assume the same amplitude within and between unit cells.

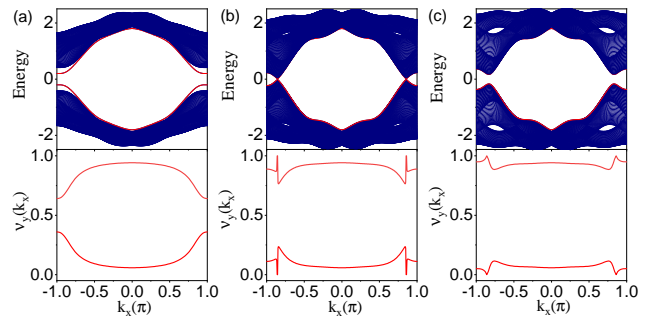


Figure 4. Edge spectrum and corresponding Wannier bands for extended model H_2 . (a) $J_2 = 0.2$. (b) $J_2 = 0.5$. Gap closure happens both at edge spectrum and Wannier bands. (c) $J_2 = 0.6$. Edge spectrum opens a gap while Wannier bands are still gapless. Other parameters are fixed at $\gamma_x = 0.8$, $\gamma_y = 0.5$ for all.

Fourier transforming H_2 to momentum space gives corresponding Bloch Hamiltonian

$$H_2(\mathbf{k}) = H_q(\mathbf{k}) + J_2(1 - \cos k_x)\Gamma_{24} + J_2 \sin k_x \Gamma_{23}, \quad (10)$$

where the Gamma matrices are defined as $\Gamma_{ab} = -i\Gamma_a\Gamma_b$. Here Γ_{24} (Γ_{23}) is odd (even) under time-reversal symmetry, thus

$$\mathcal{T}H_2(\mathbf{k})\mathcal{T}^{-1} \neq H_2(-\mathbf{k}), \quad \mathcal{T} = K, \quad (11)$$

where K represents complex conjugation. Chiral symmetry \mathcal{C} is not preserved either, while their production gives particle-hole symmetry $\mathcal{P} = \tau_3\sigma_0K$. As such, the bulk bands lose their double degeneracy, see Fig. 3(b). Crucially, the additional terms in Eq. 10 keep mirror symmetries $\mathcal{M}_{x,y}$.

Two main points are in order about the extended model $H_2(\mathbf{k})$. First, topological equivalence between edge spectrum and Wannier bands could be lost. It has been believed that Wannier bands, for instance $\nu_y(k_x)$, can be continuously mapped to the edge spectrum localized at, let us say, y -normal boundaries. But this is not necessarily true in our case. In Fig. 4(a), the edge spectrum (red lines in the top panel of Fig. 4) along x direction closes its gap as we tune J_2 to about 0.5. At this point, the Wannier bands close their gap, too. Increasing J_2 a little bit further, the edge spectrum opens a gap immediately while Wannier bands remain gapless (for a small region approximately $0.5 \lesssim J_2 \lesssim 0.65$). It is still unclear to us why the Wannier bands keep gapless for such a small parameter region, while this clearly indicates that the topological equivalence between Wannier bands and edge spectrum is lost. If J_2 is larger than about 0.65, the Wannier bands gap also opens. The discrepancy between these two bands is possible when we consider long-range hopping between unit cells, see Refs. [43, 44]. If we

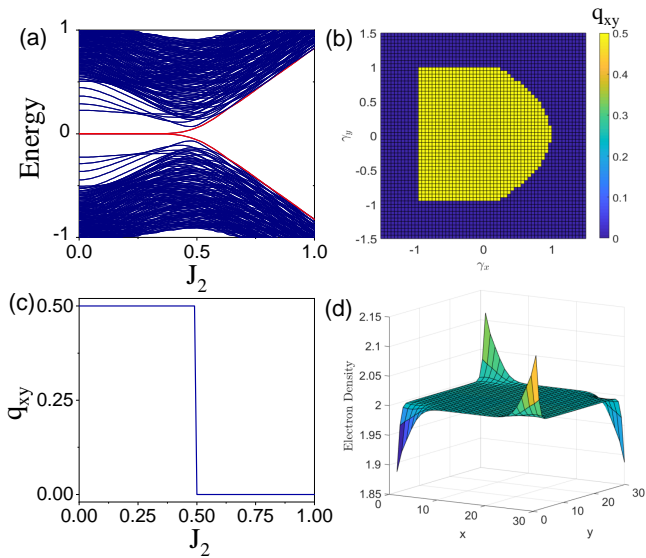


Figure 5. Topological phase transition induced by the iJ_2 hopping terms. (a) Energy spectrum as function of J_2 . We find that the zero-energy mode splits around $J_2 = 0.5$ due to topological phase transition. (b) Calculated quadrupole moments q_{xy} for fixed $J_2 = 0.5$. The nontrivial regions shrink due to topological phase transitions. (c) Numerically calculated q_{xy} corresponding to (a). Here q_{xy} jumps from one-half to zero around $J_2 = 0.5$. (d) Electron charge density in the nontrivial phase for $J_2 = 0.2$. Other parameters are fixed at $\gamma_x = 0.8, \gamma_y = 0.5$ for all. Here we set system at size 40×40 with periodic boundary for the calculation of q_{xy} .

consider edge spectrum along k_y direction, similar discrepancy happens.

The nested Wilson approach thus loses its validity to describe the topological phase. Due to the Wannier bands lose their topological equivalence with edge spectrums, it is illegal to chose a Wannier sector to calculate Berry phase of Wannier bands. Indeed, numerically calculated \mathbf{p}^v is arbitrary within $[0, 1]$ when Wannier bands keep gapless. When J_2 is larger than 0.65, the Wannier bands gap is open, while the Wannier sector polarization gives incorrect index.

Second, the edge gap close-reopen process is a topological phase transition. Note that the gap closes at two different points. Since the real phase transition happens at the sample boundaries, let us focus on the edge spectrum and ignore the Wannier bands. To show the phase transition explicitly, we employ several signatures, including quadrupole moment q_{xy} , fractional corner charges, and quantized edge polarizations. We compare the change of these signatures before and after edge spectrum closing point to make sure there is topological phase transition. Most directly, the calculation of q_{xy} jumps from $q_{xy} = 1/2$ to $q_{xy} = 0$ (see Fig. 5(c)) indicates that the edge spectrum gap close-reopen process drives quadrupole insulator from a topological nontrivial phase to trivial phase. The change of q_{xy} is associated with

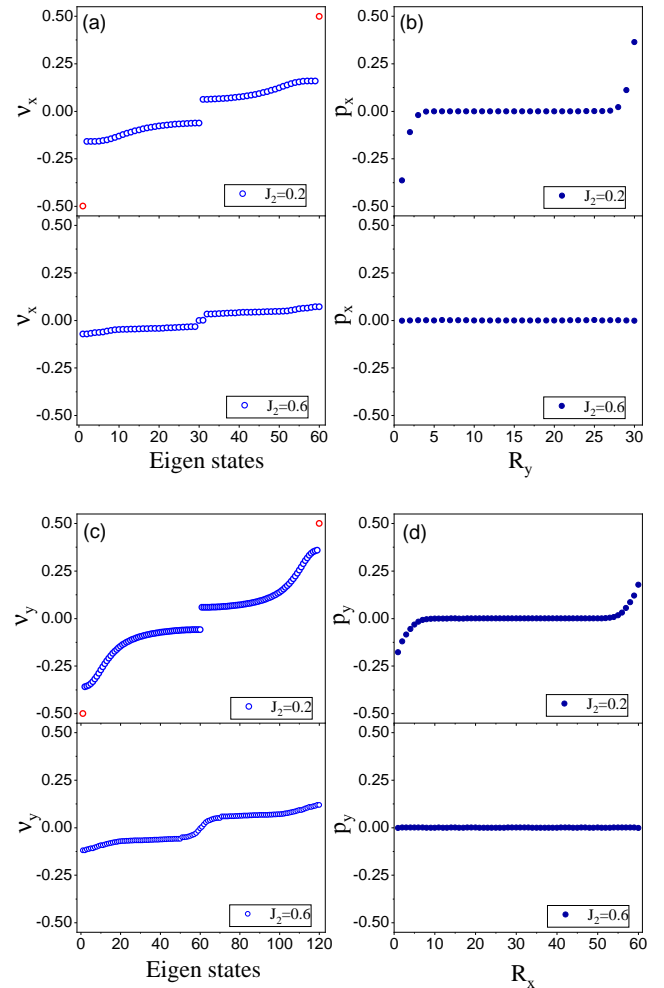


Figure 6. Wannier values and edge polarization before ($J_2 = 0.2$) and after ($J_2 = 0.6$) the topological phase transition. (a) ν_x for different eigen states, (b) edge polarization p_x along R_y , (c) ν_y for different eigen states, (d) edge polarization p_y along R_x . Other parameters are $\gamma_x = 0.8, \gamma_y = 0.5$.

the disappearance of zero-energy corner modes (see Fig. 5(a)) and fractional corner charges (see Fig. 5(d)). Before the phase transition point, the system is gapped with zero-energy corner states, as shown in Fig. 5(a). Passing over the phase transition point, no zero-energy corner modes appear in the trivial gap, which is consistent with the result of q_{xy} . The real space numerical calculations of q_{xy} turns out to be a better choice to characterize the quadrupole moments. It is clear that this topological phase transition will modify the original phase diagram. Generally, the nontrivial region will shrink, as shown in Fig. 5(b).

The edge polarization p_x^{edge} and p_y^{edge} , together with the Wannier values of states, can also help to detect the topological phase transition. Fig. 6 demonstrates the edge polarizations and Wannier centers, respectively.

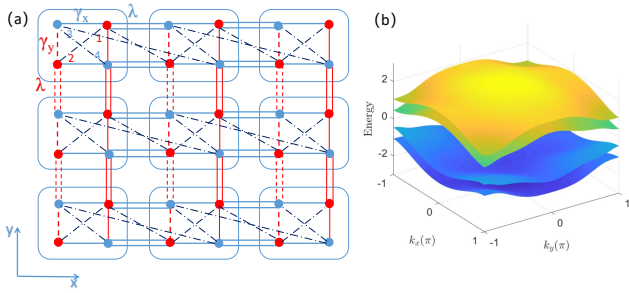


Figure 7. (a) Lattice structure of extended BBH model H_3 . The dashed dark blue lines represent hopping within and between unit cells. Here the artificial asymmetric hopping breaks mirror symmetry. (b) Energy bands corresponding to (a) with parameters fixed at $\gamma_x = \gamma_y = 0.5$, and $J_3 = 0.3$. The band degeneracy is totally lifted.

Here we stress the difference between states before and after phase transition point. The obvious signature is that: for nontrivial case where there are nonzero edge polarizations, both $p_x(R_y)$ and $p_y(R_x)$, accompanying with two isolated topological modes with pinned Wannier center $v_{x,y} = \pm 1/2$ (the red circles). Note that the edge polarizations penetrate into bulk a little bit, but their integration over half of the lattice width still gives quantized values $\pm e/2$. Whereas in the trivial case the edge polarization does not appear, neither the quantized Wannier value states.

V. ROBUST TOPOLOGICAL QUADRUPOLE PHASES UNDER MIRROR SYMMETRY BREAKING

Mirror symmetries play an important role in the BBH model to quantize quadrupole moments. Thus it is intriguing to consider the consequence of mirror symmetry breaking. To this end, we consider a model that breaks mirror symmetries explicitly, as shown in Fig. 7(a). The generalized model is

$$H_3 = H_0 + \sum_{\mathbf{R}} J_3 (iC_{\mathbf{R},2}^\dagger C_{\mathbf{R},1} - iC_{\mathbf{R},4}^\dagger C_{\mathbf{R},3} + H.c.) + \sum_{\mathbf{R}} J_3 (iC_{\mathbf{R},1}^\dagger C_{\mathbf{R}+\hat{x},2} + iC_{\mathbf{R},3}^\dagger C_{\mathbf{R}+\hat{x},4} + H.c.), \quad (12)$$

where iJ_3 is the imaginary hopping amplitude. Here we assume the same hopping amplitudes within and between unit cells for simplicity. Transforming H_3 into momentum space, it reads

$$H_3(\mathbf{k}) = H_q(\mathbf{k}) + J_3 \Gamma_{24} - J_3 (\sin k_x \Gamma_{23} - \cos k_x \Gamma_{13}). \quad (13)$$

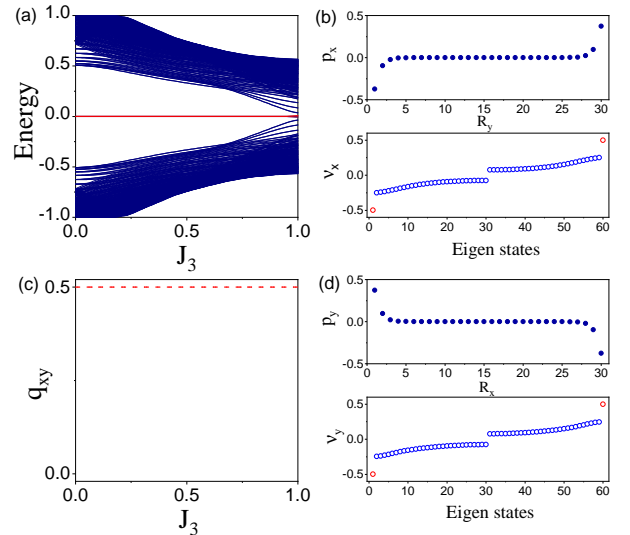


Figure 8. (a) Energy spectrum as function of J_3 . (b) ν_x for different eigen states and edge polarization p_x along R_y . (c) Numerically calculated q_{xy} corresponding to (a). (d) ν_y for different eigen states, and edge polarization p_y along R_x . Other parameters are fixed at $\gamma_x = \gamma_y = 0.5$, and $J_3 = 0.2$. Here we set system size is 40×40 with periodic boundary for the calculations of q_{xy} .

The stressed feature of $H_3(\mathbf{k})$ is the mirror symmetry breaking, which is obvious from our artificial design of hopping in Fig. 7(a). Explicitly,

$$\mathcal{M}_s H_3(\mathbf{k}) \mathcal{M}_s^{-1} \neq H_3(\mathcal{M}_s \mathbf{k}), \quad s = x, y. \quad (14)$$

The mirror symmetry operators under present basis are $\mathcal{M}_x = \tau_1 \sigma_3$, $\mathcal{M}_y = \tau_1 \sigma_1$. While $C_2 = \mathcal{M}_x \mathcal{M}_y$ rotation (resembles the inversion symmetry in this model) symmetry of $H_3(\mathbf{k})$ is preserved, which maintains the vanishing total bulk polarization to have well-defined quadrupole moments [12]. Note that chiral and time-reversal symmetries \mathcal{C} and \mathcal{T} are both absent, thus the discrepancy between edge spectrum and Wannier bands also happens here. The only preserved particle-hole symmetry puts the system into D class, whose classification is \mathbb{Z} in 2D. It is obvious from numerical result in Fig. 7(b) that the band degeneracy is totally lifted.

One remarkable result from generalized model $H_3(\mathbf{k})$ is that the topological quadrupole phases persist although mirror symmetries are absent. In the original BBH model [11, 12], the quantization of quadrupole moments is protected by combination of mirror symmetries ($H_3(\mathbf{k})$ does not respect C_4 symmetry). Here the robust topological quadrupole phases can be evidenced by several signatures. First, it is always reliable to calculate quadrupole moments q_{xy} . In Fig. 8(c), numerical results indeed show that q_{xy} quantizes at $1/2$ within present parameter regime as increasing J_3 . However, due to lacking

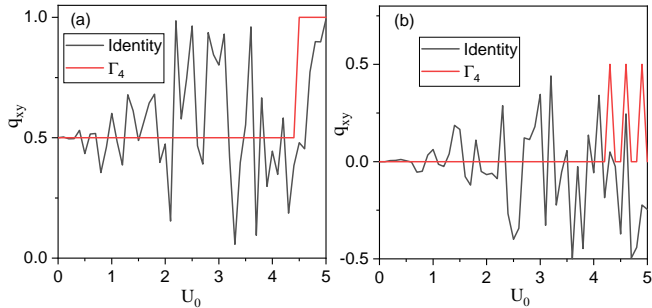


Figure 9. Quadrupole moments q_{xy} as functions of disorder strength U_0 . (a) Nontrivial case $\gamma_x = 0.8$, $\gamma_y = 0.5$; (b) trivial case with $\gamma_x = 1.5$, $\gamma_y = 0.5$. Here we set system size 50×50 with periodic boundary condition. Here we only take one disorder configuration.

of mirror symmetries, the Wannier sector polarization \mathbf{p}^ν is not quantized. Second, there are zero-energy corner modes. From the spectrum in Fig. 8(a), the red line indicates four-fold degenerate zero-energy modes, whose wave functions are sharply localized at corners of the sample. Besides, it is also found that the corner charges are fractionalized at $\pm e/2$. Third, we found that nontrivial quadrupole phase also corresponds to quantized edge polarizations. Seen from Figs. 8(b) and 8(d), two topological states localized on the edge have half-integer Wannier values, while other states are distributed over the bulk. The edge polarization $p_x(R_y)$ (or $p_y(R_x)$) shows nonzero value at the sample edge. Although they are not sharply localized at the edge sites, the integrated polarization over half of the lattice width still gives quantized edge polarization $p_x^{\text{edge}, \pm y} = \pm e/2$ ($p_y^{\text{edge}, \pm x} = \pm e/2$). Together, these signatures determine the topological quadrupole phases unambiguously.

The explanation for the robustness of q_{xy} under mirror symmetry breaking is as follows. Although mirror symmetry is used to construct the topological quadrupole insulators, it is not essentially necessary to protect for their existence. Upon mirror symmetry breaking, the robust states localized at corners persist to exist [13, 15], and more generally, their existence even does not require crystalline symmetry [57, 58].

VI. QUANTIZED QUADRUPOLE MOMENTS AGAINST DISORDERS

In this section, we investigate the disorder effect on BBH model. The topological quadrupole insulator in its essence is topological crystalline insulator, and the presence of disorder can test the robustness of topological phase. Besides, the involvement of disorder may induce more interesting topological phases, such as topological Anderson insulators [59].

Let us start with a simple on-site potential. The disorder is taken as a form $V_{dis} = V(\mathbf{R})I_{4 \times 4}$ at lattice site \mathbf{R} . Here $I_{4 \times 4}$ is identity matrix and the random on-site potential, $V(\mathbf{R})$, distributes uniformly in the interval $[-U_0/2, U_0/2]$ where U_0 is the disorder strength. Seen from Fig. 9, for quite small U_0 the quadrupole moments q_{xy} keep well-quantized. From an intuitive aspect, it is reasonable since disorder is such weak that it is considered as small perturbations. While q_{xy} fluctuates drastically as long as U_0 becomes large (comparable to bulk gap). If we perform disorder averages, the situation gets better: the quantization of quadrupole moments recover under the condition of “averaged mirror symmetry” [11]. However, it is still difficult to keep quantization of q_{xy} for much larger U_0 .

Interesting things happen when we consider another type of disorder, namely, the hopping disorder with the form $V(\mathbf{R})\Gamma_4$. In Fig. 9, we chose a specific parameter configuration to stress our points. It is shown that the quadrupole moments are well-quantized, regardless of the fact that no disorder average is made and disorder strength is very strong. The quantization of quadrupole moments is evidenced by zero-energy corner modes in the bulk gap and fractional corner charges $\pm e/2$ (not shown here). This robustness can be explained as follows. From one-dimensional point of view, the BBH model can be decomposed to two uncoupled SSH models along x and y directions, respectively. Expressed in terms of Γ matrices, $V(\mathbf{R})\Gamma_4$ type of disorder respects the chiral symmetry of SSH model along x direction. Thus the topology of each SSH model is still well-defined, regardless of presence of strong disorder [60]. Assume in the limit $U_0 \rightarrow \infty$, the system will be trivial as discussed before. The phase transition from nontrivial to trivial phase is due to the modification of mass term in the presence of strong disorder (see Appendix A). The key difference here is that the phase transition happens at boundaries. The phase diagram will be modified and even the high-order topological Anderson like phase will appear due to Γ_4 type of disorder [61]. Since our attentions in present work focus on the quantization of quadrupole moments, we focus on the fact that q_{xy} is robust even strong disorder ruins the crystalline symmetry.

VII. DISCUSSION AND CONCLUSIONS

On the one hand, nonspatial symmetries are not necessary to protect quantization of quadrupole moments, while it is shown from several generalized models that nonspatial symmetry breaking could lead to more rich topological phases to the system. On the other hand, although BBH model is constructed based on a combination of mirror symmetries, the quantized quadrupole moments and the topologically protected states at corners persist when mirror symmetry is broken. The ro-

bustness of high-order phase under symmetry breaking makes their experimental realization much easier.

Here we make a table to list the properties of several generalized models (including the original BBH model). From the symmetry analysis, only the C_2 symmetry (inversion symmetry) is necessary to assure well-defined quadrupole moments, and there is quantized quadrupole moments q_{xy} even mirror symmetry is broken.

In summary, we study the topological quadrupole phases and consequences of symmetry breaking in the

generalized BBH models. Some results here are worthy to be stressed. First, nested Wilson loop approach is not suitable to characterize the high-order topology of the generalized models, and real space formula for quadrupole moments turns out to be useful; second, the topological equivalence between Wannier bands and edge spectrum could be lost; third, quantized quadrupole moments and the topologically protected boundary signatures continue to exist when mirror symmetry is broken or in the presence of disorder.

Table I. Symmetries and properties of the quantized quadrupole insulator models.

	\mathcal{M}_x	\mathcal{M}_y	C_2	C_4	\mathcal{C}	\mathcal{T}	\mathcal{P}	$q_{xy} = 0, 1/2$	Quantized p^{edge}
$H_0(\mathbf{k})$	✓	✓	✓	✓	✓	✓	✓	✓	✓
$H_1(\mathbf{k})$	✓	✓	✓	✓	×	✓	×	✓	✓
$H_2(\mathbf{k})$	✓	✓	✓	×	×	×	✓	✓	✓
$H_3(\mathbf{k})$	×	×	✓	×	×	×	✓	✓	✓

VIII. ACKNOWLEDGMENTS

C.-A. Li thanks B. Fu, Z.-A. Hu, J. Li, and S.-Q. Shen for helpful discussions, and thanks SUSTech, China for hospitality at the initial stage of this project. This work is supported by foundation of Westlake University.

- [1] R. Resta, Rev. Mod. Phys. **66**, 899 (1994).
- [2] R. Resta, Phys. Rev. Lett. **80**, 1800 (1998).
- [3] R. D. King-Smith and D. Vanderbilt, Phys. Rev. B **47**, 1651 (1993).
- [4] M. Z. Hasan and C. L. Kane, Rev. Mod. Phys. **82**, 3045 (2010).
- [5] X.-L. Qi and S.-C. Zhang, Rev. Mod. Phys. **83**, 1057 (2011).
- [6] S.-Q. Shen, Topological Insulators: Dirac Equation in Condensed Matter, 2nd ed. (Springer, Singapore, 2017).
- [7] B. A. Bernevig and T. L. Hughes, Topological insulators and topological superconductors (Princeton University Press, 2013).
- [8] D. J. Thouless, Phys. Rev. B **27**, 6083 (1983).
- [9] L. Fu and C. L. Kane, Phys. Rev. B **74**, 195312 (2006).
- [10] W. P. Su, J. R. Schrieffer, and A. J. Heeger, Phys. Rev. Lett. **42**, 1698 (1979).
- [11] W. A. Benalcazar, B. A. Bernevig, and T. L. Hughes, Science **357**, 61 (2017).
- [12] W. A. Benalcazar, B. A. Bernevig, and T. L. Hughes, Phys. Rev. B **96**, 245115 (2017).
- [13] L. Trifunovic and P. W. Brouwer, Phys. Rev. X **9**, 011012 (2019).
- [14] F. Schindler, A. M. Cook, M. G. Vergniory, Z. Wang, S. S. P. Parkin, B. A. Bernevig, and T. Neupert, Science Advances **4** 6 (2018).
- [15] J. Langbehn, Y. Peng, L. Trifunovic, F. von Oppen, and P. W. Brouwer, Phys. Rev. Lett. **119**, 246401 (2017).
- [16] E. Khalaf, Phys. Rev. B **97**, 205136 (2018).
- [17] Z. Song, Z. Fang, and C. Fang, Phys. Rev. Lett. **119**, 246402 (2017).
- [18] M. Geier, L. Trifunovic, M. Hoskam, and P. W. Brouwer, Phys. Rev. B **97**, 205135 (2018).
- [19] I. Petrides and O. Zilberberg, (2019), arXiv:1911.08461 [cond-mat.mes-hall].
- [20] Z. Wang, B. J. Wieder, J. Li, B. Yan, and B. A. Bernevig, Phys. Rev. Lett. **123**, 186401 (2019).
- [21] F. Schindler, Z. Wang, M. G. Vergniory, A. M. Cook, A. Murani, S. Sengupta, A. Y. Kasumov, R. Deblock, S. Jeon, I. Drozdov, H. Bouchiat, S. Gueon, A. Yazdani, B. A. Bernevig, and T. Neupert, Nature Physics **14**, 918 (2018).
- [22] M. Serra-Garcia, V. Peri, R. Sustrunk, O. R. Bilal, T. Larsen, L. G. Villanueva, and S. D. Huber, Nature **555**, 342 (2018).
- [23] C. W. Peterson, W. A. Benalcazar, T. L. Hughes, and G. Bahl, Nature **555**, 346 (2018).
- [24] S. Franca, J. van den Brink, and I. C. Fulga, Phys. Rev. B **98**, 201114 (2018).
- [25] Z. Yan, F. Song, and Z. Wang, Phys. Rev. Lett. **121**, 096803 (2018).
- [26] Q. Wang, C.-C. Liu, Y.-M. Lu, and F. Zhang, Phys. Rev. Lett. **121**, 186801 (2018).
- [27] C.-H. Hsu, P. Stano, J. Klinovaja, and D. Loss, Phys. Rev. Lett. **121**, 196801 (2018).

- [28] Y. Volpez, D. Loss, and J. Klinovaja, Phys. Rev. Lett. **122**, 126402 (2019).
- [29] T. Liu, J. J. He, and F. Nori, Phys. Rev. B **98**, 245413 (2018).
- [30] X. Zhu, Phys. Rev. B **97**, 205134 (2018).
- [31] H. Shapourian, Y. Wang, and S. Ryu, Phys. Rev. B **97**, 094508 (2018).
- [32] M. Ezawa, Phys. Rev. Lett. **120**, 026801 (2018).
- [33] R. Okugawa, S. Hayashi, and T. Nakanishi, (2019), arXiv:1907.01153 [cond-mat.mes-hall].
- [34] B. J. Wieder, Z. Wang, J. Cano, X. Dai, L. M. Schoop, B. Bradlyn, and B. A. Bernevig, (2019), arXiv:1908.00016 [cond-mat.mes-hall].
- [35] L. Fu, Phys. Rev. Lett. **106**, 106802 (2011).
- [36] T. Neupert and F. Schindler, “Topological crystalline insulators,” in Topological Matter: Lectures from the Topological Matter School 2017, edited by D. Bercioux, J. Cayssol, M. G. Vergniory, and M. Reyes Calvo (Springer International Publishing, Cham, 2018) pp. 31–61.
- [37] A. Yoshida, Y. Otaki, R. Otaki, and T. Fukui, Phys. Rev. B **100**, 125125 (2019).
- [38] E. Khalaf, H. C. Po, A. Vishwanath, and H. Watanabe, Phys. Rev. X **8**, 031070 (2018).
- [39] R. Yu, X. L. Qi, A. Bernevig, Z. Fang, and X. Dai, Phys. Rev. B **84**, 075119 (2011).
- [40] L. Fidkowski, T. S. Jackson, and I. Klich, Phys. Rev. Lett. **107**, 036601 (2011).
- [41] A. Alexandradinata, X. Dai, and B. A. Bernevig, Phys. Rev. B **89**, 155114 (2014).
- [42] E. Khalaf, W. A. Benalcazar, T. L. Hughes, and R. Queiroz, (2019), arXiv:1908.00011 [cond-mat.meshall].
- [43] Y.-B. Yang, K. Li, L. M. Duan, and Y. Xu, (2019), arXiv:1910.04151 [cond-mat.mes-hall].
- [44] Y.-B. Yang, K. Li, and Y. Xu, (2019), arXiv:1910.14189 [cond-mat.mes-hall].
- [45] A. P. Schnyder, S. Ryu, A. Furusaki, and A. W. W. Ludwig, Phys. Rev. B **78**, 195125 (2008).
- [46] C.-K. Chiu, J. C. Y. Teo, A. P. Schnyder, and S. Ryu, Rev. Mod. Phys. **88**, 035005 (2016).
- [47] B.-H. Chen and D.-W. Chiou, (2017), arXiv:1705.06913 [cond-mat.mes-hall].
- [48] L. Li, Z. Xu, and S. Chen, Phys. Rev. B **89**, 085111 (2014).
- [49] B. Perez-Gonzalez, M. Bello, A. Gomez-Leon, and G. Platero, (2018), arXiv:1802.03973 [cond-mat.meshall].
- [50] B. Kang, K. Shiozaki, and G. Y. Cho, Phys. Rev. B **100**, 245134 (2019).
- [51] W. A. Wheeler, L. K. Wagner, and T. L. Hughes, Phys. Rev. B **100**, 245135 (2019).
- [52] B. Roy, (2019), arXiv:1906.10685 [cond-mat.mes-hall].
- [53] S. Ono, L. Trifunovic, and H. Watanabe, Phys. Rev. B **100**, 245133 (2019).
- [54] C.-A. Li, S.-B. Zhang, and S.-Q. Shen, Phys. Rev. B **97**, 045420 (2018). [55] R. Skolasinski, D. I. Pikulin, J. Alicea, and M. Wimmer, Phys. Rev. B **98**, 201404 (2018).
- [55] R. Skolasinski, D. I. Pikulin, J. Alicea, and M. Wimmer, Phys. Rev. B **98**, 201404 (2018).
- [56] F. D. M. Haldane, Phys. Rev. Lett. **61**, 2015 (1988).
- [57] S.-B. Zhang and B. Trauzettel, (2019), arXiv:1905.09308 [cond-mat.supr-con].
- [58] Y. You, (2019), arXiv:1908.04299 [cond-mat.str-el].
- [59] J. Li, R.-L. Chu, J. K. Jain, and S.-Q. Shen, Phys. Rev. Lett. **102**, 136806 (2009).
- [60] I. Mondragon-Shem, T. L. Hughes, J. Song, and E. Prodan, Phys. Rev. Lett. **113**, 046802 (2014).
- [61] C.-A. Li, et. al., unpublished.

Appendix A: The effective model

Let us derive an effective Hamiltonian from BBH model. For the chosen parameters, the bulk gap of BBH model close at (π, π) point when $\gamma_x = \gamma_y = 1$. Expanding Eq. 2 at this gap closing point to the second order, we have an effective model

$$H_{\text{eff}}(\mathbf{k}) = \begin{pmatrix} 0 & Q \\ Q^\dagger & 0 \end{pmatrix},$$

$$Q \equiv -m_x \sigma_0 - ik_x \sigma_3 - im_y \sigma_2 - ik_y \sigma_1, \quad (\text{A1})$$

where $m_x \equiv 1 - \gamma_x - k_x^2/2$, and $m_y \equiv 1 - \gamma_y - k_y^2/2$. Note that this effective Hamiltonian inherits all symmetries of the original BBH model. After proper rotation of Gamma matrices, we arrive at

$$H_{\text{eff}}(\mathbf{k}) = m_x \beta + \alpha \cdot \mathbf{p}, \quad (\text{A2})$$

where the Dirac matrices are defined as $\beta = \tau_3 \sigma_0$, and $\alpha_i = \tau_1 \sigma_i$. The “momentums” in Eq. A2 are defined as

$$\mathbf{p} \equiv (k_y, m_y, k_x). \quad (\text{A3})$$

Here we recover the fact that this effective model Eq. A2 is exactly Dirac equation in two-dimension [6], whereas one of the momentums is replaced by mass term m_y . Tracing back the relation between Γ_i matrices before rotation and $\{\beta, \alpha\}$ Dirac matrices in Eq. A2, we find that $\Gamma_4 \rightarrow \beta$. This means that the disorder of the form $V(\mathbf{R})\Gamma_4$ modifies the mass term of Dirac Hamiltonian Eq. A2. Besides, it explains why the quadrupole is still quantized when strong disorder is applied, as shown in Fig. 9, to some extent.

Actually, Eq. A2 describes the same physics as quantum spin Hall insulator with an edge gap term. This point would be transparent if the Dirac matrices are rotated by a unitary transformation

$$\begin{pmatrix} \alpha'_2 \\ \beta' \end{pmatrix} = \frac{1}{\sqrt{2}} \begin{pmatrix} 1 & -1 \\ 1 & 1 \end{pmatrix} \begin{pmatrix} \alpha_2 \\ \beta \end{pmatrix}. \quad (\text{A4})$$

For simplicity, let us set $\gamma_x = \gamma_y = \gamma$. With the help of Eq. A4, the effective model is transformed to

$$H_{\text{eff}}(\mathbf{k}) = m(\mathbf{k})\beta' + k_x \alpha_3 + k_y \alpha_1 + \Delta(\mathbf{k})\alpha'_2, \quad (\text{A5})$$

$$m(\mathbf{k}) \equiv \left[\sqrt{2}(1 - \gamma) - \frac{k^2}{2\sqrt{2}} \right], \Delta(\mathbf{k}) \equiv \frac{k_x^2 - k_y^2}{2\sqrt{2}}. \quad (\text{A6})$$

From the mass term $m(\mathbf{k})$, the system is topologically nontrivial when $\gamma < 1$, which is consistent with BBH

model. Note that the rotated Dirac matrices still obey Clifford algebra. If $\Delta(\mathbf{k}) = 0$, which is only satisfied if $k_x^2 = k_y^2$, the effective Hamiltonian describes quantum spin Hall insulator. Generally, $\Delta(\mathbf{k})$ acts as a mass term to gap helical edge modes as it anticommutes with other Dirac matrices in the Eq. A5, and it creates a domain wall profile since it changes sign at adjacent two edges. In this sense, the BBH model is equivalent to a quantum spin Hall insulator with an anisotropic edge gap term.

Appendix B: Calculation details

Here we show the details about the calculation of nested Wilson loop approach and edge polarization [11, 12]. The nested Wilson loop approach is based on Wilson loop, thus let us start with the construction of Wilson loop. The Wilson loop operator parallel to y direction is constructed as

$$\hat{P}_{y,\mathbf{k}} = P_{N_y \delta k_y + k_y} P_{(N_y - 1) \delta k_y + k_y} \cdots P_{\delta k_y + k_y} P_{k_y}, \quad (\text{B1})$$

where each projection operator is defined as $P_{m \delta k_y + k_y} \equiv \sum_{n \in N_{\text{occ}}} |u_{k_x, m \delta k_y + k_y}^n\rangle \langle u_{k_x, m \delta k_y + k_y}^n|$ with $|u_{k_x, m \delta k_y + k_y}^n\rangle$ being the n -th eigen state of occupied bands at point $(k_x, m \delta k_y + k_y)$, and m is an integer taking values from $\{1, 2, \dots, N_y\}$. The projection method can avoid the arbitrary phase problem in numerical realizations. Here N_y is the number of unit cells, n is the band index, and N_{occ} is the number of occupied bands. Note that $\hat{P}_{y,\mathbf{k}}$ has dimension of N now with N being the total bands number. After projection onto the occupied bands at base point \mathbf{k} , there is $N_{\text{occ}} \times N_{\text{occ}}$ matrix $\mathcal{W}_{y,\mathbf{k}}$ that defines a Wannier Hamiltonian $H_{\mathcal{W}_y}(\mathbf{k})$ from the relation $\mathcal{W}_{y,\mathbf{k}} = \exp[iH_{\mathcal{W}_y}(\mathbf{k})]$. The eigen values of $H_{\mathcal{W}_y}(\mathbf{k})$ give the Wannier bands $2\pi\nu_y(k_x)$ associated with eigen states $|\nu_{y,\mathbf{k}}^j\rangle$, $j \in \{1, 2, \dots, N_{\text{occ}}\}$. Similar procedure is applicable for the construction of $\mathcal{W}_{x,\mathbf{k}}$.

These Wannier bands can carry their own topology and have associated Berry phases. If the Wannier bands are gapped, then one can chose a Wannier sector and construct nested Wilson loop $\widetilde{\mathcal{W}}_{x,k_y}$ by the similar projection procedures as before, which gives rise Wannier section polarization $p_x^{v_y}$. To this end, we need to define the Wannier basis

$$|w_{y,\mathbf{k}}^\ell\rangle = \sum_n^{N_{\text{occ}}} |u_{\mathbf{k}}^n\rangle [\nu_{y,\mathbf{k}}^\ell]^n, \quad (\text{B2})$$

where ℓ takes value from set $\{1, 2, \dots, N_{\text{ws}}\}$, and N_{ws} is the dimension of chosen Wannier sector. Here $[\nu_{y,\mathbf{k}}^\ell]^n$ is the n -th component of eigen state $|\nu_{y,\mathbf{k}}^\ell\rangle$. The nested Wilson loop operator parallel along x direction is constructed as

$$\hat{P}_{x,\mathbf{k}} = \mathcal{P}_{N_x \delta k_x + k_x} \mathcal{P}_{(N_x - 1) \delta k_x + k_x} \cdots \mathcal{P}_{\delta k_x + k_x} \mathcal{P}_{k_x}, \quad (\text{B3})$$

where each projection operator is defined as $\mathcal{P}_{q \delta k_x + k_x} \equiv \sum_{\ell=1}^{N_{\text{ws}}} |w_{y,q \delta k_x + k_x, k_y}^\ell\rangle \langle w_{x,q \delta k_x + k_x, k_y}^\ell|$ where q is also an integer taking values from set $\{1, 2, \dots, N_x\}$. Note that $\hat{P}_{x,\mathbf{k}}$ also has dimension of N now. After projection onto the Wannier basis of chosen sector, there is $N_{\text{ws}} \times N_{\text{ws}}$ matrix $\widetilde{\mathcal{W}}_{x,k_y}$ that defines a nested Wilson loop. The polarization of Wannier bands is given as

$$p_x^{v_y} = \frac{1}{2\pi i N_y} \sum_{k_y} \log \det \widetilde{\mathcal{W}}_{x,k_y}. \quad (\text{B4})$$

Similar procedure can be carried out for the construction of $p_y^{v_x}$.

The edge polarization is exhibited on ribbon samples with finite width but infinite length [12]. It is a useful signature to exhibit high-order topology in quadrupole insulators. Let us assume the ribbon is infinite along x direction. First, we treat the width along y as inner degree of freedom and get Wannier band $v_{k_x}^s$ using projection method described as above. The associated wave functions are $|\nu_{k_x}^s\rangle$ where $s \in \{1, 2, \dots, N_{\text{tot}}\}$ where $N_{\text{tot}} = N_y \times N_{\text{occ}}$. Second, we construct hybrid Wannier function as

$$|\Psi_{R_x}^s\rangle = \frac{1}{\sqrt{N_x}} \sum_{k_x} \sum_{n=1}^{N_{\text{tot}}} [v_{k_x}^s]^n e^{-ik_x R_x} \Upsilon_{n,k_x}^\dagger |0\rangle, \quad (\text{B5})$$

where Υ_{n,k_x} is the basis that diagonalizes the Hamiltonian. One can check that $|\Psi_{R_x}^s\rangle$ is a complete basis such that $\langle \Psi_{R_x}^s | \Psi_{R_x}^{s'} \rangle = \delta_{ss'}$. Third, we consider the probability distribution of the Wannier function along y direction

$$\begin{aligned} \rho^s(R_y) &= \sum_{R'_x, \zeta} \langle \Psi_{R_x}^s | \phi_{R'_x}^{R_y, \zeta} \rangle \langle \phi_{R'_x}^{R_y, \zeta} | \Psi_{R_x}^s \rangle, \\ |\phi_{R'_x}^{R_y, \zeta}\rangle &= \sum_{k_x} e^{-ik_x R'_x} C_{k_x, R_y, \zeta}^\dagger |0\rangle, \end{aligned} \quad (\text{B6})$$

where ζ denotes the inner degree of freedom at each unit cell. Finally, the edge polarization along x direction is

$$p_x(R_y) = \sum_{s=1}^{N_{\text{tot}}} \rho^s(R_y) v_{k_x}^s. \quad (\text{B7})$$

The total edge polarization p_x^{edge} is defined as summation of $p_x(R_y)$ over half of the width along y direction.

The corner charge is another direct signature of high-order topology of quadrupole insulators. The local charge density is

$$\rho(R_x, R_y) \equiv e \sum_{n=1}^{N_{\text{occ}}} \sum_{\zeta=1}^4 |u^n(R_x, R_y, \zeta)|^2, \quad (\text{B8})$$

where $u^n(R_x, R_y, \zeta)$ is the component of n -th eigen state $|u^n\rangle$. The corner charge is defined as the summation of

charge density over a quarter of the sample, for instance,

$$Q^{\text{corner},-x,-y} = \sum_{R_x=1}^{N_x/2} \sum_{R_y=1}^{N_y/2} [\rho(R_x, R_y) - 2e]. \quad (\text{B9})$$

Note that here we need to eliminate contributions from the atomic charge $2e$.